Applied Radiation and Isotopes 67 (2009) 1842–1854

Contents lists available at ScienceDirect

Applied Radiation and Isotopes

journal homepage: www.elsevier.com/locate/apradiso

A comprehensive evaluation of charged-particle data for production of the therapeutic radionuclide ^{103}Pd

M. Hussain [a,b], S. Sudar [b], M.N. Aslam [a,b], H.A. Shah [a], R. Ahmad [a], A.A. Malik [a], S.M. Qaim [c,*]

[a] Department of Physics, Government College University Lahore, Lahore 54000, Pakistan
[b] Institute of Experimental Physics, University of Debrecen, H-4001 Debrecen, Hungary
[c] Institut für Nuklearchemie, Forschungszentrum Jülich GmbH, D-52425 Jülich, Germany

ARTICLE INFO

Article history:
Received 10 February 2009
Received in revised form
16 June 2009
Accepted 29 June 2009

Keywords:
^{103}Pd
Charged-particle-induced reaction
Excitation function
Nuclear model calculation
Data evaluation
Production yield calculation

ABSTRACT

^{103}Pd is an important radionuclide having a half-life of 16.99 d, which is suitable for internal radiation therapy, especially used for the treatment of prostate cancer. Its production in no-carrier-added form is done via charged-particle-induced reactions and the data are available in EXFOR library. We evaluated six charged-particle-induced reactions, namely ^{nat}Ag(p,x)^{103}Pd, ^{103}Rh(p,n)^{103}Pd, ^{103}Rh(d,2n)^{103}Pd, ^{100}Ru(α,n)^{103}Pd, ^{101}Ru(α,2n)^{103}Pd, and ^{102}Ru(^{3}He,2n)^{103}Pd process. In the first case, analysis was done up to about 100 MeV but in other cases only up to about 25 or 40 MeV. Furthermore, an evaluation of the data for the ^{nat}Ag(p,x)^{103}Ag process was also done since it may serve as a typical example for the ^{103}Ag→^{103}Pd precursor system. A statistical procedure supported by nuclear model calculations using the codes STAPRE, EMPIRE 2.19, and TALYS was used to validate and fit the experimental data. The recommended sets of data derived together with confidence limits are reported. The application of those data, particularly in the calculation of integral yields, is discussed. A comparison of the investigated routes from the viewpoint of practical applicability to the production of ^{103}Pd is given. Presently the ^{103}Rh(p,n)^{103}Pd reaction is the method of choice.

1. Introduction

The significance of internal radionuclide therapy is increasing (cf. Hoefnagel, 1991; Stöcklin et al., 1995), and the role of nuclear data in efficient production and application of suitable radionuclides has been discussed (cf. Qaim, 2001). ^{103}Pd is an important therapeutic radionuclide. It has a half-life of 16.99 d and decays to ^{103m}Rh ($T_{1/2}$ = 56.1 min) by electron capture (EC), which further de-excites through internal transition (IT). The consequence of EC and IT is the emission of X-rays and Auger electrons, which makes this radionuclide suitable for internal radiotherapy. In every 100 decays of ^{103}Pd, 80 X-rays, 186 Auger electrons, and 95 low-energy conversion electrons are emitted (NuDat 2.4 database). ^{103}Pd is mostly used as a seed or stent for the treatment of prostate cancer.

For the production of ^{103}Pd, neutron, photon, and charged-particle-induced reactions have been attempted. The irradiation of Pd with neutrons makes use of the ^{102}Pd(n,γ)^{103}Pd reaction but the achieved specific activity is very low, particularly due to the low abundance of 1.02% of the target isotope ^{102}Pd in natural Pd. Some attempts are underway to produce ^{103}Pd using highly enriched ^{102}Pd and high neutron fluxes, but high specific activity is yet to be demonstrated. Another route worth considering is the ^{104}Pd(γ,n)^{103}Pd process since the target has comparatively higher abundance (11.14%) but here also it remains to be shown whether the desired high specific activity would be achieved. Today, the routine production of ^{103}Pd is done via the ^{103}Rh(p,n)^{103}Pd reaction using a cyclotron. In USA alone, for the production of ^{103}Pd, over the last 10 years about 30 small-sized but high-intensity cyclotrons have been installed (cf. Qaim, 2004).

The charged-particle-induced reactions, in general, lead to ^{103}Pd in no-carrier-added form, and thus the product is of high specific activity. Seven major routes considered for the production of ^{103}Pd in no-carrier-added form were taken into account in this work. They include proton-, deuteron-, ^{3}He-, and α-particle-induced reactions on various target nuclei. For each reaction a critical evaluation of the excitation function was done. Therefrom recommended reaction cross-section values for the production of ^{103}Pd were deduced. The experimental data were validated by modern nuclear model calculations.

A recent study on therapeutic radionuclides under the auspices of a Co-ordinated Research Project (CRP) of the IAEA has also dealt with the evaluation of cross-sections of a few reactions leading to the formation of ^{103}Pd in no-carrier-added form (cf. Capote et al., 2008; Qaim et al., 2009). The present work entails a much more detailed study; it incorporates not only many more reactions but

* Corresponding author. Tel.: +49 2461 613282; fax: +49 2461 612535.
E-mail address: s.m.qaim@fz-juelich.de (S.M. Qaim).

0969-8043/$ - see front matter © 2009 Elsevier Ltd. All rights reserved.
doi:10.1016/j.apradiso.2009.06.010

also presents results of two nuclear model calculations (STAPRE and TALYS) not previously attempted in the IAEA-CRP work.

2. Normalization and selection of the experimental data

All available data for seven important charged-particle-induced reactions up to incident particle energy of 100 MeV, used in the production of ^{103}Pd, were collected (EXFOR database). The contributing nuclear reactions, their *Q*-values, and the relevant references are given in Table 1. For each nuclear reaction, decay data and monitor reaction cross-section data, when given in original publications, were compared with the latest accepted data for normalization of the experimental data. No normalization was done when the difference was less than 5%, since we report 95% confidence limits in the recommended data. Also in the measurements where neutrons were detected, no normalization factors were applied. The decay data of ^{103}Pd were taken from Nudat 2.4 database. For each reaction, nuclear model calculations were done (see below) and the ratio of the measured/model calculated cross-section was developed. We fitted this ratio using a polynomial function with weighting errors to estimate the energy-dependent normalization factor. It was assumed that cross-sections are functions of model calculations and the energy-dependent factor.

To estimate the best fit, we neglected the data that were out of 3σ limit of the uncertainties of the polynomial fit. After neglecting those data, polynomial fittings were done again by taking into account the weighting factor of the uncertainties. The normalization factor for each model calculation was estimated and multiplied by the model calculation; 95% confidence limits were selected to estimate the uncertainty in the recommended data. This technique allowed us to remove major energy dependence of the cross-section (not completely because the polynomial fits of the ratios were not simple linear functions of the first order). Recommended sets of the data were generated by taking average and average fit of the three normalized model calculations. The evaluated curves have a difference of about 5% in comparison with the model calculations.

Table 1
Investigated nuclear processes for the production of ^{103}Pd, *Q*-values, and references.

Nuclear reaction	*Q*-values (MeV)	References
^{nat}Ag(p,x)^{103}Pd[a], including		Fassbender et al. (1999), Uddin et al. (2005), Uddin et al. (2008)
^{107}Ag(p,αn)^{103}Pd	−4.13	
^{107}Ag(p,p4n)^{103}Ag→^{103}Pd	−35.90	
^{107}Ag(p,5n)^{103}Cd→^{103}Ag→^{103}Pd	−40.82	
^{109}Ag(p,α3n)^{103}Pd	−20.59	
^{109}Ag(p,p6n)^{103}Ag→^{103}Pd	−52.36	
^{109}Ag(p,7n)^{103}Cd→^{103}Ag→^{103}Pd	−57.29	
^{103}Rh(p,n)^{103}Pd	−1.33	Blaser et al. (1951), Albert (1959), Johnson et al. (1960), Harper et al. (1961), Hansen, Albert (1962), Mukhammedov and Vasidov (1984), Hermanne et al. (2000), Sudár et al. (2002)
^{103}Rh(d,2n)^{103}Pd	−3.55	Hermanne et al. (2002a, b)
^{100}Ru(α,n)^{103}Pd	−7.39	Skakun and Qaim (2005, 2008)
^{101}Ru(α,2n)^{103}Pd	−14.19	Skakun and Qaim (2005, 2008)
^{102}Ru(^{3}He,2n)^{103}Pd	−2.83	Skakun and Qaim (2005, 2008)

[a] Composition of ^{nat}Ag: ^{107}Ag (51.839%), ^{109}Ag (48.161%).

3. Nuclear models

Nuclear model calculations are an integral part of modern nuclear data evaluation methodology. Several calculational codes have been developed that are helpful in the validation of existing data; they can generate an evaluation that is entirely complete in its description of reaction channels, and incident and outgoing particle energies and angles. The adjustable parameters of the nuclear model code should be fitted to reproduce the experimental data in the process of evaluation. The most important parameters and mechanisms are optical model parameters, compound nucleus formation, direct interactions, level density parameters, gamma-ray transmission coefficients, pre-equilibrium reactions, and multiple emissions of particles.

3.1. Nuclear model calculations using STAPRE

This is one of the oldest codes and was developed at Vienna by Uhl and Strohmaier (1976). It has been extensively used for data validation under Jülich–Debrecen collaboration (Sudár and Qaim, 1996, 2006; Nesaraja et al., 2003). The extensions of the code refer to the exciton model and Hauser–Feshbach formula for γ-rays in the exit channels. The pre-equilibrium emission was taken into account by the exciton model formalism while for the compound part the width-fluctuation-corrected Hauser–Feshbach formula was used. Direct interactions were not considered since their contributions were estimated to be $<10\%$. The spherical optical model was used to produce the transmission coefficients of the particles; this was done by using the computer code SCAT 2 (cf. Bersillon, 1981). The optical model parameters used were: for neutron, Wilmore and Hodgson (1964); for proton, Perey (1963) after adjustment and modification; and for alpha particles, McFadden and Satchler (1966). For all nuclear reactions the deuteron optical model potential of Perey (1963) was adopted. In the case of ^{3}He-paticles, the OMP of Becchetti and Greenlees (1969) was used.

Primarily two particles and one hole approach was used for exciton model calculations to describe the precompound part. IT rates were calculated by using Pauli's principle. The square of absolute value of the effective matrix element for two-body residual interactions was calculated by the formula proposed by Kalbach-Cline (1973). FM has been treated as an adjustable parameter. For first chance γ-ray emission in cascade, two compound nuclei were considered. For the maximum multipolarity of γ-rays, the Brink–Axel model and Weisskopf model were used to account for E_1, M_1; E_2, M_2; and E_3, M_3 radiations. The levels were treated by back-shifted Fermi gas model (BFM) proposed by Dilg et al. (1973). The adopted levels for the excited states of product nuclei were described according to the data available in the form of ENDSF data files of Brookhaven National Laboratory, USA (2008). For level density parameter the RIPL-2 library of the IAEA was consulted and parameterization was also done according to the systematics of Egidy and Bucurescu (2005). The rigid body moment of inertia was used to account for the spin distribution of the level densities. The data for the spin and parities of the target nuclei and non-standard projectile were collected from the National Nuclear Data Center, Brookhaven National Laboratory, USA (2008).

3.2. Nuclear model calculations using EMPIRE

EMPIRE is a nuclear model code developed by Herman et al. (2007). It is an empire of codes that work for different calculational tasks during a complete nuclear model calculation. For our calculations we used the spherical optical model. This was done by the ECIS-03 code (cf. Raynal, 2003), which calculates the

elastic scattering and direct reactions induced by the light particles $A \leq 4$ in the frame of the generalized optical model. It made use of the RIPL-2 library (Belgya et al., 2006) for the optical model segment and for discrete levels. The population of discrete and collective levels occurs in the inelastic scattering. This was calculated within the coupled channel (CC) mode. The calculation takes into account the ground state and the coupled levels. By this consideration, transmission coefficients were calculated for pre-equilibrium emissions. The transmission coefficients define the absorption cross-section that is available for the pre-equilibrium decay. The reaction cross-sections were then attained by the sum of direct cross-sections to collective levels and the absorption cross-sections. In calculations the EMPIRE-specific level density parameters and Gilbert and Cameron (1965) level densities were used; the pre-equilibrium modules used were the same as defined in the literature (Herman et al., 2007).

For protons incident on ^{103}Rh, the exciton model calculations were done with the code PCROSS; cluster emission was considered in terms of the Iwamoto and Harada (1982) model and the mean free path parameter in PCROSS was set to 2.0. Gilbert and Cameron (1965) level densities were selected; the number of energy steps in the integration was set to 100. The optical model parameters for emitted particles were set to RIPL-2. For deuterons incident on ^{103}Rh, EMPIRE-specific level densities were selected and the number of energy steps in the integration was again set to 100. The level density parameter a in ^{104}Pd was multiplied by 0.9. GDR parameters were from RIPL-2/Plujko systematics.

For alpha particles incident on ^{100}Ru and ^{101}Ru, the EMPIRE-specific level densities were selected and the number of energy steps in the integration was set to 100. MSC calculations were also selected; GDR parameters were from RIPL-2/Plujko systematics. For ^{3}He particles incident on ^{102}Ru, all the parameters were similar to those for previous cases. The level density parameter a for ^{105}Pd was multiplied by 1.2 and that for ^{103}Pd by 0.9.

3.3. Nuclear model calculations using TALYS

TALYS is a computer code system developed at NRG Petten and CEA for the prediction and analysis of nuclear reactions (Koning et al., 2005). TALYS can do the nuclear model calculations for the reactions that involve neutrons, γ-rays, protons, deuterons, tritons, hellions, and alpha particles. The energy range it covers is from 1 keV to 200 MeV.

TALYS produces a complete set of nuclear data of the investigated reaction. The output of the nuclear reaction involves total, elastic, and non-elastic cross-sections; elastic scattering angular distributions; inelastic scattering cross-sections and angular distributions to discrete levels; exclusive channel cross-sections, total particle cross-sections, and double differential spectra; γ-ray production; and isomeric, ground state, and residual production cross-sections. The optical model calculations in TALYS were done by the code ECIS-06 based on Koning and Delaroche (2003) with automatic χ^2 optimization of optical model potentials, but the assessments were used only to initialize OMP parameters.

We adjusted the OMP parameters for proton-induced reactions and modified the parameters of the OMP for alpha- and ^{3}He-particle-induced reactions. For alpha particles incident on ^{100}Ru, *rvadjust* was set to 1.09 and *Cstrip* was taken to be 1.2. For alpha particles incident on ^{101}Ru, *avdadjust, avadjust*, *rvadjust*, and *rvdadjust* were set to 1.12, 1.15, 0.8, and 1.11, respectively. For ^{3}He particles incident on ^{102}Ru, *rvadjust* and *Cstrip* were set to 1.11 and 1.2 respectively. By default, in TALYS, light-ion emissions at higher energies were also considered. All the parameterization was done within the recommended ranges. All nuclei were considered nearly spherical in shape. The compound nucleus contribution was considered in the frame of the Hauser–Feshbach model. The contributions of direct reactions were taken into account by DWBA. For level densities, the back-shifted Fermi gas model was used, in which the pairing energy was taken as an adjustable parameter. Energy-dependent shell effects were also considered.

4. Evaluation of proton-induced reactions

Proton beams of specified energies incident on ^{103}Rh or ^{nat}Ag have been used to produce no-carrier-added ^{103}Pd. The nuclear processes include ^{103}Rh(p,n)^{103}Pd and ^{nat}Ag(p,x)^{103}Pd. The formation of ^{103}Ag, a precursor of ^{103}Pd, has also been investigated via several nuclear routes. We concentrated here on the evaluation of the above-mentioned two reactions leading to the direct or cumulative formation of ^{103}Pd. The ^{103}Ag$\rightarrow$ ^{103}Pd precursor route is discussed below separately (see Section 8).

The nuclear reaction ^{103}Rh(p,n)^{103}Pd was investigated by several groups (see below), but the experimental measurements and a critical analysis of the data for this reaction reported by Sudár et al. (2002) appear to be the most comprehensive. Treytl and Caretto (1966) measured the data for the same reaction between 100 and 400 MeV. Due to very high energy, those data have not been included in this evaluation. Fassbender et al. (1999) investigated the ^{nat}Ag(p,x)^{103}Pd reaction up to 100 MeV and Uddin et al. (2005) up to 80 MeV.

4.1. ^{nat}Ag(p,x)^{103}Pd reaction

Natural silver consists of ^{107}Ag (51.84%) and ^{109}Ag (48.16%). Its interaction with protons has been investigated mostly at high energies (greater than 100 MeV) but some work has also been carried out at lower energies. Fassbender et al. (1999) proposed an alternative production route for ^{103}Pd using natural silver foils as target, combined with chemical separation and determination of the radioactivity via high-resolution X-ray spectrometry. Investigations were done up to 100 MeV proton energy using the stacked-foil technique. The monitor reaction ^{27}Al(p,x)^{22}Na was used to measure the beam current. Since its adopted cross-section agreed within 5% of the recommended monitor cross-section (IAEA-TECDOC-1211), no normalization of the data was done. The uncertainty in measured cross-sections was estimated as 25%. Similarly, Uddin et al. (2005) measured cross-sections for the production of ^{103}Pd and several other radionuclides in the interaction of silver with protons of energies between 51 and 80 MeV. They did not measure the X-rays. Instead, they relied on the very weak γ-ray at 357.4 keV (0.0221%). The proton flux was measured carefully using several monitor reactions; so no normalization was done. The results of the two experimental measurements are given in Fig. 1. Evidently four data points from Fassbender et al. (1999) and three data points from Uddin et al. (2005) fall rather away from the general trend. In a communication with the present authors Uddin et al. (2005) alluded to large errors in the three data points between 60 and 80 MeV. Those data points are therefore regarded as discrepant. The other data points reported by the two groups via two different radioactivity assay methods are in agreement within the limits of uncertainties.

The production of ^{103}Pd can take place via many channels, the possible processes being ^{107}Ag(p,αn)^{103}Pd, ^{107}Ag(p,p4n)^{103}Ag$\rightarrow$ ^{103}Pd,^{107}Ag(p,5n)^{103}Cd$\rightarrow$ ^{103}Ag$\rightarrow$ ^{103}Pd, ^{109}Ag(p,α3n)^{103}Pd, ^{109}Ag (p,p6n)^{103}Ag$\rightarrow$ ^{103}Pd, and ^{109}Ag(p,7n)^{103}Cd$\rightarrow$ ^{103}Ag$\rightarrow$ ^{103}Pd. In nuclear model calculations we considered all those processes and the results are shown in Fig. 1 together with the experimental data. At higher energies light complex particles (deuteron and

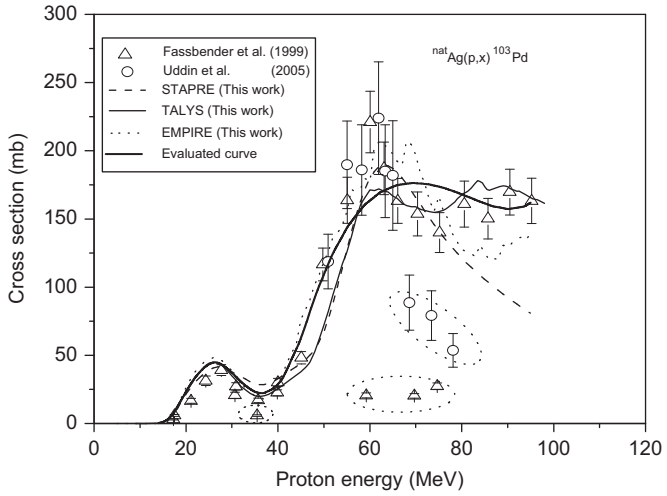

Fig. 1. Experimental data for the $^{nat}Ag(p,x)^{103}Pd$ reaction in comparison with the results of nuclear model calculations. The encircled data points were not considered in deducing the evaluated curve, shown as a solid line.

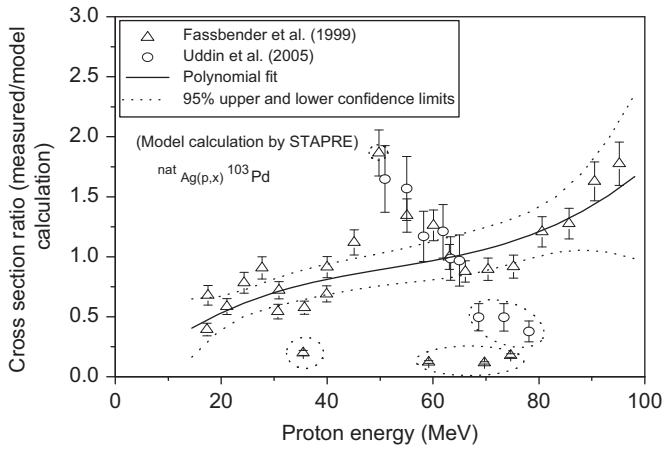

Fig. 2. Cross-section ratio of the experimental data to model calculations by STAPRE.

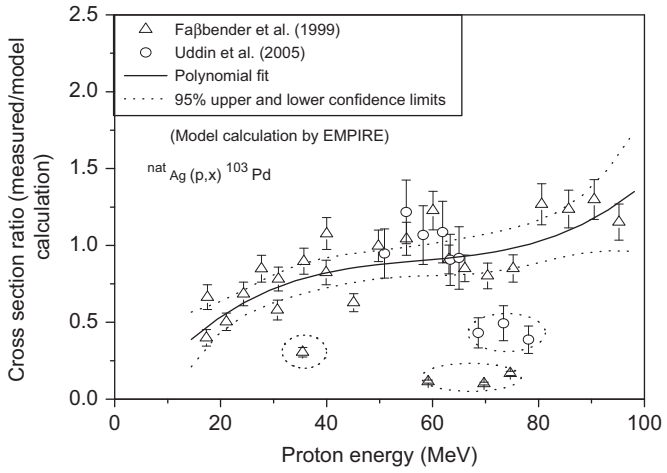

Fig. 3. Cross-section ratio of the experimental data to model calculations by EMPIRE.

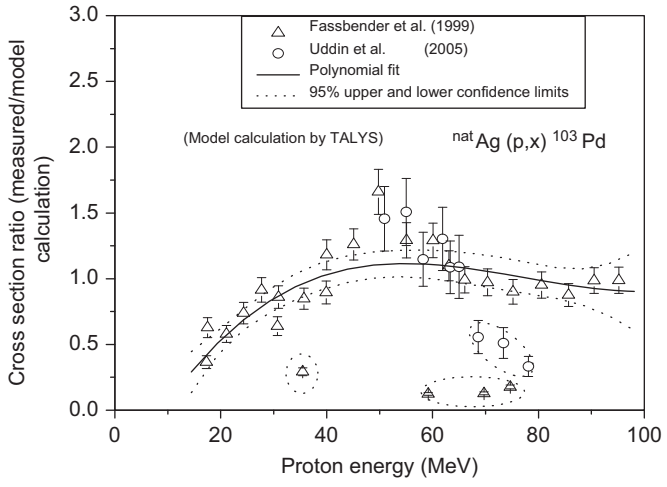

Fig. 4. Cross-section ratio of the experimental data to model calculations by TALYS.

triton) may also be emitted. They were not taken into account in the STAPRE and EMPIRE 2.19 calculations; so those theoretical calculations above 80 MeV are lower than the TALYS calculations, which reproduce the experimental data well. Up to 30 MeV and between 60 and 80 MeV, on the other hand, the three calculations are in agreement with the experimental data; but between 30 and 60 MeV the EMPIRE results are rather high. Thus in general terms, the three codes validate the experimental data fairly well, though in certain energy ranges some deviations are observed.

For producing a set of recommended data for practical applications, we did polynomial fitting to the ratio data for each model calculation (Figs. 2–4.). This way the data that were found beyond 3σ limit were neglected; they have been encircled. The recommended sets of data were then generated, and upper and lower 95% confidence limits are reported for the best estimation of uncertainty in the recommended values, which are given in Table 2.

4.2. $^{103}Rh(p,n)^{103}Pd$ reaction

The most commonly used nuclear process for production of ^{103}Pd is the $^{103}Rh(p,n)^{103}Pd$ reaction. The status of nuclear data for this reaction was reviewed (Sudár et al., 2002). Measurements have been done via emitted neutron spectroscopy as well as by characterization of the activation product. Large amounts of data exist in the literature; eight experiments were considered and the data after normalization (wherever necessary) are shown in Fig. 5. Three experiments were done via neutron counting and five via assay of the ^{103}Pd activity. We discuss them in some detail.

Albert (1959) obtained seven data points up to 9 MeV. The proton current was monitored to about 2% accuracy and neutrons emitted from the target were measured with an instrumental error of about 10%. The values at 7 and 8.1 MeV were very inconsistent and much higher as compared with other data. Later Hansen and Albert (1962) measured six cross-section values up to 10 MeV using the same technique. The data followed the other experimental work, and theoretical calculations reproduced the data very well. Johnson et al. (1960) also used the neutron detection technique and reported 27 cross-section values between 2 and 6 MeV at a Van de Graaff accelerator; the data were low in comparison with those of nuclear theory. The total uncertainty was estimated to be about 10%. The neutron measurements were thus limited up to proton energies of 10 MeV, thereby avoiding (p,xn) reactions.

Regarding identification of the activation product ^{103}Pd, Blaser et al. (1951) reported for the first time 10 data points up to 7 MeV using stacked-target irradiation. However, no information about error estimation was given; so we assumed 10% uncertainty in the

Table 2
Recommended sets of data for the $^{nat}Ag(p,x)^{103}Pd$ reaction.

Energy (MeV)	σ (mb)	95% confidence limits		Energy (MeV)	σ (mb)	95% confidence limits	
		Lower	Upper			Lower	Upper
15.0	1.12	1.06	1.17	42.0	39.9	33.3	44.9
15.5	1.84	1.75	1.93	43.0	47.2	40.5	53.1
16.0	2.92	2.77	3.07	44.0	54.6	47.6	61.2
16.5	4.38	4.16	4.6	45.0	62.1	54.9	69.7
17.0	6.4	6.1	6.7	46.0	72.2	63.5	81.1
17.5	8.6	8.2	9.0	47.0	82.2	72.1	92.5
18.0	11.4	10.9	12.0	48.0	92.2	80.7	104
18.5	14.2	13.5	14.9	49.0	101	88.4	114
19.0	17.4	16.5	18.3	50.0	109	95.4	123
19.5	20.3	19.2	21.3	51.0	117	102	132
20.0	23.6	22.4	24.8	52.0	125	109	141
20.5	26.2	24.9	27.5	53.0	131	115	148
21.0	28.9	27.5	30.4	54.0	137	120	155
21.5	31.3	29.7	32.8	55.0	143	125	161
22.0	33.8	32.1	35.5	56.0	148	130	167
22.5	35.8	34.0	37.5	57.0	152	133	172
23.0	37.8	35.9	39.7	58.0	157	137	176
23.5	39.4	37.5	41.4	59.0	161	141	181
24.0	41.1	39.1	43.2	60.0	163	143	184
24.5	42.4	40.3	44.5	61.0	166	146	187
25.0	43.6	41.4	45.8	62.0	169	148	190
25.5	44.2	41.9	46.4	63.0	171	150	192
26.0	44.7	42.5	46.9	64.0	172	151	194
26.5	44.7	42.4	46.9	65.0	174	152	195
27.0	44.6	42.4	46.9	66.0	175	153	197
27.5	43.7	41.6	45.9	67.0	175	154	197
28.0	42.9	40.7	45.0	68.0	176	154	198
28.5	41.5	39.5	43.6	69.0	176	154	198
29.0	40.2	38.2	42.2	70.0	176	154	198
29.5	38.7	36.8	40.6	72.0	176	154	198
30.0	37.2	35.3	39.0	74.0	174	152	197
31.0	33.9	32.2	35.6	76.0	173	150	196
32.0	30.4	28.9	31.9	78.0	171	147	194
33.0	27.6	26.3	29.0	80.0	168	144	192
34.0	25.2	23.9	26.4	82.0	165	140	191
35.0	23.2	22.0	24.3	84.0	163	136	189
36.0	22.3	21.2	23.4	86.0	160	132	188
37.0	22.3	21.2	23.4	88.0	159	129	188
38.0	23.9	22.7	25.1	90.0	157	126	189
39.0	25.7	24.4	27.0	92.0	158	123	193
40.0	28.8	27.3	30.2	94.0	160	122	198
41.0	32.8	31.2	34.5				

reported cross-section values. Harper et al. (1961) measured the data radiochemically up to 22 MeV. The Major sources of uncertainties were beam monitoring, chemical yield, and counting normalization. The overall uncertainty in absolute values was estimated to be up to 15%. Their data were consistent but the data around 20 MeV were lower than the other data and theoretical calculations.. Mukhammedov and Vasidov (1984) measured the data up to 17 MeV using sedimented Rh layers on thin Al backing, in contrast with metallic foils used in previous works. The results obtained showed deviations in the low-energy region. In all the three activation measurements the ^{103}Pd activity was determined via gross X/γ-ray counting. Since no details on the intensity of the radiation and the adopted proton flux monitor reaction were given, any normalization of the data could not be done.

Hermanne et al. (2000) studied the production of ^{103}Pd and characterized the possible contaminants during proton irradiation of 99.9% pure ^{103}Rh up to 28 MeV. Seven stacks of the target material and monitor foils were irradiated with 14.7, 22.5, and 29.4 MeV proton beams. The monitor reactions were $^{nat}Cu(p,x)^{65}Zn$, $^{nat}Ni(p,x)^{57}Ni$, and $^{nat}Ti(p,x)^{48}V$. The monitor reference data agree with the latest recommended values (IAEA-TECDOC-1211). We therefore did not normalize those data. Measurements were done using the weak γ-ray of energy 357.4 keV along with the X-rays, and there was a difference of 25% in the cross-section values.

Sudár et al. (2002) performed the measurements very carefully using 99.9% pure Rh foils. Four stacks were irradiated with 12.0, 15.8, 19.6, and 45.1 MeV proton beams. The beam current was monitored by $^{63}Cu(p,n)^{63}Zn$ and $^{65}Cu(p,n)^{65}Zn$ reactions, and the reference data were taken from Collé et al. (1974) and Kopecky (1985), respectively. The data of the latter reaction are in agreement with the IAEA-TECDOC-1211 values but in the former case there are deviations up to 20–25%. Since in the energy region above 20 MeV, mostly the $^{nat}Cu(p,x)^{65}Zn$ monitor reaction was used, no normalization of the data was done. In the energy region below 20 MeV, however, the data of the monitor reaction $^{63}Cu(p,n)^{63}Zn$ were normalized to the IAEA-TECDOC-1211 values. This led to an increase in the $^{103}Rh(p,n)^{103}Pd$ reaction cross-sections by 5–10%. Sudár et al. (2002) reported 26 values of the reaction cross-section up to 40 MeV. It was recommended explicitly that emphasis should be placed on measurements done using X-rays, since the cross-section values obtained by counting the weak γ-ray at 357.4 keV were considered unreliable.

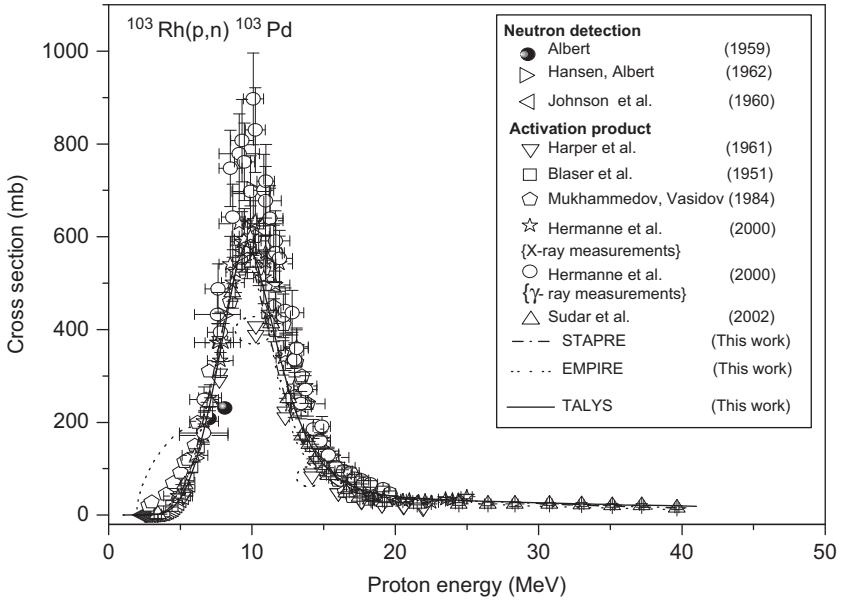

Fig. 5. Experimental data for the $^{103}Rh(p,n)^{103}Pd$ reaction in comparison with the results of nuclear model calculations.

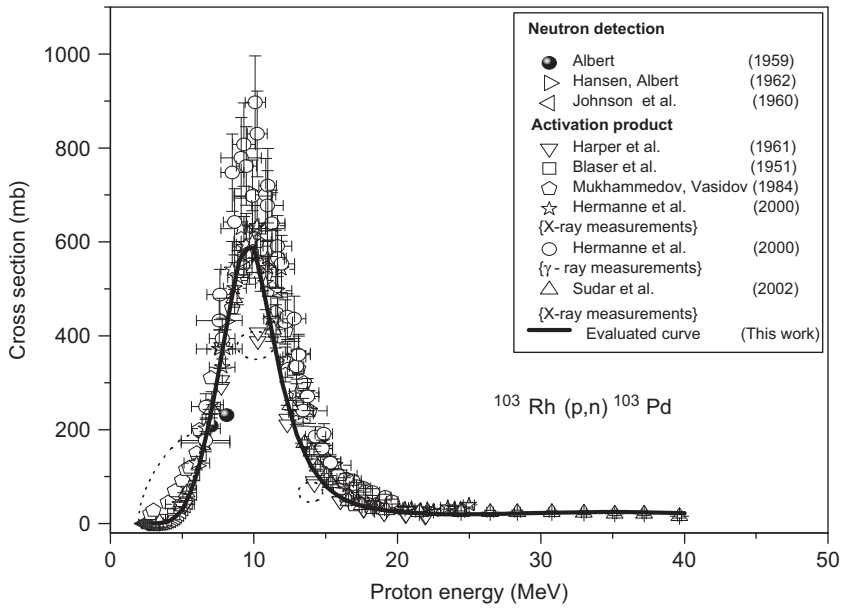

Fig. 6. Experimental data for the ^{103}Rh(p,n)^{103}Pd reaction. In deducing the evaluated curve, shown as a solid line, the encircled data points as well the data obtained using the weak 357.4 keV γ-ray were not considered.

After analyzing all the experimental data we performed nuclear model calculations using the three above-mentioned codes. Above 20 MeV, the three nuclear model calculations have a deviation of about 10% in comparison with the evaluated curve. The results are shown in Fig. 5. Nuclear theory reproduced the experimental data very well except for the peak values of the cross-section. We did polynomial fitting to the ratio data for each model calculation (see above). The data of Mukhammedov and Vasidov (1984) and of Harper et al. (1961) that fell outside the 3σ uncertainties of the fit were not considered for the evaluation (encircled data). The data of Hermanne et al. (2000) obtained via γ-ray measurement and some X-ray data that fell outside the 3σ uncertainties of the fit were also deselected. The recommended sets of data were generated, and 95% upper and lower confidence limits were established for the best estimation of uncertainty in the recommended values. Considering the importance of this reaction we give the evaluated curve separately in Fig. 6. The numerical values are given in Table 3. A comparison of our recommended data with the ongoing CRP (Qaim et al., 2009) data shows that over the energy region up to about 7 MeV our values are up to 10% lower, in the energy range 7–10 MeV up to 25% higher, in the energy range 11–24 MeV up to 25% lower, and in the energy range 24–40 MeV up to 100% higher. On the other hand, the cross-section above 24 MeV is relatively small so that in absolute terms the deviations may be regarded as not too significant, the CRP values being within the 95% confidence limits of our data.

5. Evaluation of deuteron-induced reactions

The deuteron-induced reactions investigated for the production of ^{103}Pd include ^{103}Rh(d,2n)^{103}Pd and ^{nat}Pd(d,x)^{103}Pd. The latter process gives only carrier-added ^{103}Pd; so it was neglected. Measurements were also done on the ^{nat}Pd(d,x)^{103}Ag process with the aim to develop the ^{103}Ag→^{103}Pd precursor system (Hermanne et al., 2004). Furthermore, Uddin et al. (2006) performed some experimental studies on deuteron-induced reactions on ^{nat}Ag, but they did not report the production of ^{103}Pd or ^{103}Ag. We therefore concentrated only on the ^{103}Rh(d,2n) process. The ^{103}Ag→^{103}Pd precursor route is discussed below separately (see Section 8).

Table 3
Recommended sets of data for the ^{103}Rh(p,n)^{103}Pd reaction.

Energy (MeV)	σ (mb)	95% confidence limits		Energy (MeV)	σ (mb)	95% confidence limits	
		Lower	Upper			Lower	Upper
3.0	0.21	0.19	0.22	17.0	42	40	44
3.5	1.48	1.41	1.56	17.5	38	36	40
4.0	4.16	3.96	4.36	18.0	34	32	36
4.5	14.0	13.4	14.6	18.5	31	29	33
5.0	29	28	30	19.0	29	27	30
5.5	63	60	65	19.5	27	25	28
6.0	104	100	108	20.0	25	23	27
6.5	166	160	172	21.0	23	21	25
7.0	235	226	244	22.0	21	19	23
7.5	318	306	330	23.0	20	17	23
8.0	405	390	420	24.0	20	16	23
8.5	486	468	504	25.0	20	16	24
9.0	561	541	582	26.0	20	15	25
9.5	584	563	606	27.0	21	15	26
10.0	588	567	609	28.0	21	16	27
10.5	523	504	542	29.0	22	16	28
11.0	448	432	465	30.0	23	16	29
11.5	372	358	385	31.0	23	16	30
12.0	297	286	308	32.0	24	16	31
12.5	242	233	251	33.0	24	17	32
13.0	189	182	196	34.0	25	17	33
13.5	154	147	160	35.0	25	16	33
14.0	121	116	126	36.0	24	16	33
14.5	99	95	104	37.0	24	15	34
15.0	80	77	84	38.0	25	13	34
15.5	68	65	71	39.0	23	12	34
16.0	57	54	59	40.0	22	9	35
16.5	49	47	51				

5.1. ^{103}Rh(d,2n)^{103}Pd reaction

Measurements on the formation of ^{103}Pd via this reaction were done only by Hermanne et al. (2002a, b) using the stacked-foil technique. The beam current was monitored by the ^{nat}Ti(d,x)^{48}V reaction. The total uncertainties were up to 10%. Since standard decay data and monitor reaction cross-sections were used, no normalization was done. Measurements were carried out using the X-rays as well as the weak γ-ray with energy E_γ = 357.4 keV.

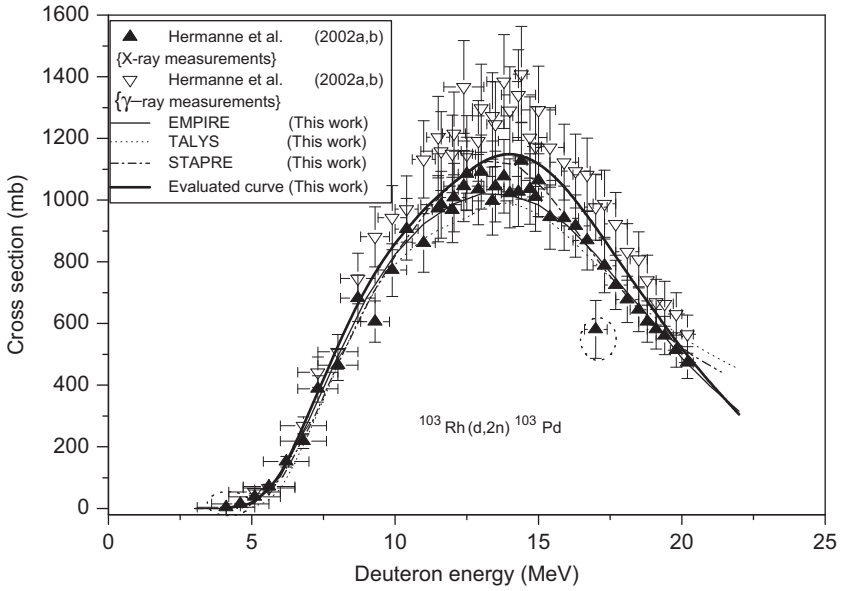

Fig. 7. Experimental data for the ^{103}Rh(d,2n)^{103}Pd reaction in comparison with the results of nuclear model calculations. The encircled data points as well as the data obtained using the weak 357.4 keV γ-ray were not considered in deducing the evaluated curve.

The data are shown in Fig. 7. Similar to the (p,n) reaction on ^{103}Rh described above, also for the (d,2n) reaction on ^{103}Rh the γ-ray spectrometry gave higher cross-sections than the X-ray spectrometry. We did the nuclear model calculations using the above-mentioned three codes.

At low energies nuclear model calculations reproduced the experimental data successfully. A difference of only 5% was found around 5 MeV. The calculations by TALYS were about 10% lower than the other two calculations and the evaluated curve below 6 MeV. In the region between 12 and 15 MeV, where most of the data were found, the cross-sections obtained using the γ-ray spectroscopic analysis were about 20% higher, reaching values of about 1300 mb. In the region above 15 MeV, nuclear theory followed the data with a shift of 1 MeV. We did polynomial fitting to the ratio data for each model calculation (see above). In the fitting process only the data obtained via X-ray analysis were considered. The cross-sections that were found beyond 3σ limit have been encircled. The recommended sets of data were generated, and upper and lower 95% confidence limits were determined for the best estimation of uncertainty in the recommended values. The recommended sets of data are given in Table 4. They are somewhat lower around the threshold and up to 5.5 MeV but in general about 5–10% higher than the recommended data of the ongoing CRP (Qaim et al., 2009).

After we had submitted this manuscript for publication, we received a preprint (Tárkányi et al., 2009) describing some more measurements on this reaction. The three new data points in the energy range up to 22 MeV agree within the limits of uncertainties with the recommended data given in this work. However, since the higher-energy region (up to 40 MeV) is not of direct relevance to the production of ^{103}Pd, we did not extend our calculations to that region.

6. Evaluation of alpha-particle-induced reactions

Production of ^{103}Pd using alpha particles was also investigated but the available data are very limited (Skakun and Qaim, 2005, 2008).

Table 4
Recommended sets of data for the ^{103}Rh(d,2n)^{103}Pd reaction.

Energy (MeV)	σ (mb)	95% confidence limits		Energy (MeV)	σ (mb)	95% confidence limits	
		Lower	Upper			Lower	Upper
4.0	0.30	0.23	0.33	13.5	1143	1101	1185
4.5	6.6	5.7	7.4	14.0	1152	1109	1195
5.0	15	13	16	14.5	1142	1097	1186
5.5	55	49	60	15.0	1120	1074	1166
6.0	107	97	116	15.5	1082	1036	1127
6.5	207	190	223	16.0	1035	989	1079
7.0	310	289	330	16.5	974	931	1017
7.5	420	394	445	17.0	913	872	953
8.0	528	498	558	17.5	843	805	881
8.5	627	592	662	18.0	776	741	811
9.0	718	679	758	18.5	709	674	744
9.5	794	751	836	19.0	646	610	682
10.0	861	816	906	19.5	581	540	622
10.5	916	870	962	20.0	519	471	567
11.0	970	923	1016	20.5	462	404	519
11.5	1013	968	1058	21.0	407	338	476
12.0	1055	1011	1098	21.5	355	275	435
12.5	1088	1046	1131	22.0	305	215	396
13.0	1123	1082	1165				

6.1. ^{100}Ru (α,n)^{103}Pd reaction

This reaction was studied via the stacked-foil technique using 95.8% enriched ^{100}Ru as target material (Skakun and Qaim, 2005, 2008). Samples were prepared by electrolytic deposition. The activity of the product was measured via X-ray spectrometry. The beam current was measured using α-particle-induced reactions on Cu monitor foils, for which the cross-sections were taken from Gul et al. (2001). This eliminated the necessity of normalization of data. The measured data are given in Fig. 8.

The experimental data are consistent, and at 17.3 MeV the excitation function reaches the maximum cross-section value of 555 mb. The nuclear model calculations were again done using STAPRE, EMPIRE 2.19, and TALYS codes. They all give a peak near 17 MeV and the overall shape of the excitation function is in good agreement with the experimental data. Only one data point at the

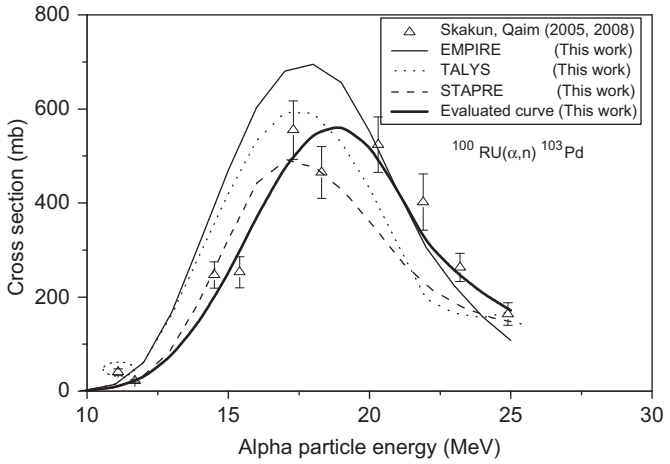

Fig. 8. Experimental data for the ^{100}Ru(α,n)^{103}Pd reaction in comparison with the results of nuclear model calculations. The encircled data point was not considered in deducing the evaluated curve, which is shown by a solid line.

Table 5
Recommended sets of data for the ^{100}Ru(α,n)^{103}Pd reaction.

Energy (MeV)	σ (mb)	95% confidence limits		Energy (MeV)	σ (mb)	95% confidence limits	
		Lower	Upper			Lower	Upper
10.0	1.7	0.4	3.0	18.0	547	422	672
10.5	5.0	2.0	8.0	18.5	556	423	689
11.0	8.0	4.0	14	19.0	565	425	705
11.5	19	11	27	19.5	543	404	682
12.0	29	18	41	20.0	521	384	658
12.5	53	33	72	20.5	473	349	599
13.0	76	49	103	21.0	426	314	540
13.5	113	72	154	21.5	372	276	469
14.0	151	96	205	22.0	318	238	399
14.5	201	133	268	22.5	287	215	361
15.0	250	170	331	23.0	256	191	322
15.5	310	221	399	23.5	232	167	299
16.0	370	272	467	24.0	208	142	275
16.5	423	320	526	24.5	190	113	268
17.0	476	368	584	25.0	171	83	260
17.5	512	395	628				

lowest energy, i.e. 11.1 MeV, with the corresponding cross-section value of 40.5 mb, seems to be higher than the calculated values. At higher energies the calculational results appear to be shifted to lower energies by about 2 MeV. We did polynomial fitting to the ratio data for each model calculation. Only the 11.1 MeV cross-section value was found beyond 3σ limit; it has been encircled. The recommended sets of data were generated, and upper and lower 95% confidence limits were determined for the best estimation of uncertainty in the recommended values. The recommended sets of data are given in Table 5.

6.2. ^{101}Ru(α,2n)^{103}Pd reaction

Cross-section measurements on this reaction were also done via the stacked-foil technique using 97.6% enriched ^{101}Ru as target material (Skakun and Qaim, 2005, 2008). The experimental data are shown in Fig. 9. The beam current monitoring was done as described above, so no normalization was necessary. The reported uncertainties in cross-sections are rather high— above 21 MeV; the total uncertainty in cross-section increased up to about 10% but the yield expected via this reaction is much higher than that via the ^{100}Ru(α,n)^{103}Pd reaction. This reaction may be interesting if high-energy α-particles are available, because the theoretical calculations predict increasing cross-section values at energies higher than 24 MeV. The results of nuclear model calculations employing the codes STAPRE, EMPIRE 2.19, and TALYS are also shown in Fig. 9. The EMPIRE 2.19 calculations reproduced the experimental data very well but TALYS and STAPRE gave lower cross-section values, although the overall shape of the experimental excitation function agrees with the theoretical calculations. We did polynomial fitting to the ratio data for each model calculation (see above). No data point was found beyond 3σ limit; so we kept all the data for evaluation. The recommended sets of data were generated, and 95% upper and lower confidence limits were determined for the best estimation of uncertainty in the recommended values. The recommended sets of data are given in Table 6.

7. Evaluation of ^{102}Ru(^{3}He,2n)^{103}Pd reaction

For studying this reaction, 99% enriched ^{102}Ru was used as target material and the measurements were done using the

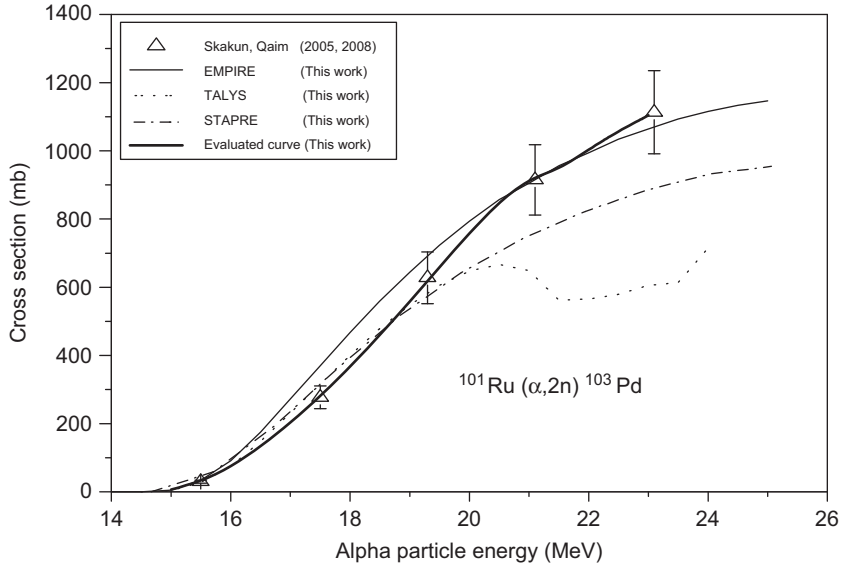

Fig. 9. Experimental data for the ^{101}Ru(α,2n)^{103}Pd reaction in comparison with the results of nuclear model calculations. The evaluated curve is shown by a solid line.

Table 6
Recommended sets of data for the ^{101}Ru(α,2n)^{103}Pd reaction.

Energy (MeV)	σ (mb)	95% confidence limits		Energy (MeV)	σ (mb)	95% confidence limits	
		Lower	Upper			Lower	Upper
15.0	6.7	3.3	10	20.0	759	599	920
15.5	30	19	41	20.5	850	658	1042
16.0	72	51	94	21.0	919	704	1134
16.5	132	96	168	21.5	945	719	1171
17.0	202	147	257	22.0	1004	781	1228
17.5	280	206	354	22.5	1058	832	1285
18.0	366	277	454	23.0	1104	822	1387
18.5	459	359	559	23.5	1122	728	1559
19.0	558	446	670	24.0	1184	742	1855
19.5	659	527	791				

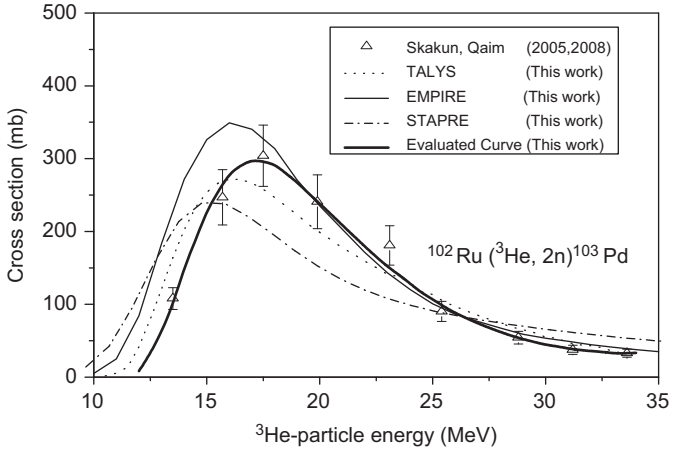

Fig. 10. Experimental data for the ^{102}Ru(^{3}He,2n)^{103}Pd reaction in comparison with the results of nuclear model calculations. The evaluated curve is shown by a solid line.

stacked-foil technique (Skakun and Qaim, 2005, 2008). The ^{3}He-particle beam current was measured via the reaction induced in Ti monitor foils. The monitor reaction used had a good status, with a difference of only 5% from the cross-section values recommended in Gul et al. (2001). The cross-sections have uncertainties as described above. The energy range covered was from 13.5 to 35 MeV. The experimental data are shown in Fig. 10. The maximum value of the reaction cross-section was observed at about 17 MeV. The nuclear model calculations were done using the above-mentioned three codes. Nuclear theory predicted the data well, especially in the case of EMPIRE 2.19 and TALYS, but with a shift of about 2 MeV to lower energy in the low-energy region. The cross-section values above 30 MeV show some deviations from the model calculations. We did polynomial fitting to the ratio data for each model calculation. No data point was found beyond 3σ limit; so we kept all the data for evaluation. The recommended sets of data were generated, and upper and lower 95% confidence limits were determined for the best estimation of uncertainty in the recommended values. The recommended sets of data are given in Table 7.

8. Evaluation of ^{103}Ag→^{103}Pd precursor route

The formation of ^{103}Ag has been investigated in five nuclear processes, namely ^{nat}Pd(p,x)^{103}Ag (Hermanne et al., 2004; Tárkányi et al., 2009), ^{nat}Pd(d,x)^{103}Ag (Hermanne et al., 2004), ^{nat}Pd(α,x)^{103}Ag (Hermanne et al., 2005), ^{nat}Ag(p,x)^{103}Ag (Uddin et al., 2008), and ^{nat}Cd(p,x)^{103}Ag (Tárkányi et al., 2009). We scrutinized all the data.

Table 7
Recommended sets of data for the ^{102}Ru(^{3}He,2n)^{103}Pd reaction.

Energy (MeV)	σ(mb)	95% confidence limits		Energy (MeV)	σ(mb)	95% confidence limits	
		Lower	Upper			Lower	Upper
12.0	8	2	26	23.5	141	123	160
12.5	33	17	60	24.0	129	112	146
13.0	63	37	89	24.5	116	101	132
13.5	99	79	132	25.0	107	92	122
14.0	150	125	176	25.5	97	83	111
14.5	187	162	219	26.0	88	75	101
15.0	229	197	260	26.5	81	68	94
15.5	255	221	290	27.0	74	62	86
16.0	280	242	317	27.5	68	57	79
16.5	291	251	330	28.0	62	51	73
17.0	298	257	339	28.5	57	47	67
17.5	296	255	337	29.0	52	43	62
18.0	293	252	333	29.5	48	40	57
18.5	280	241	319	30.0	45	37	53
19.0	268	231	305	30.5	42	35	50
19.5	252	218	287	31.0	39	32	46
20.0	238	206	271	31.5	37	30	44
20.5	224	194	254	32.0	36	29	43
21.0	209	181	236	32.5	35	27	42
21.5	194	169	220	33.0	33	25	40
22.0	179	156	202	33.5	33	24	41
22.5	165	144	187	34.0	33	23	43
23.0	152	132	171				

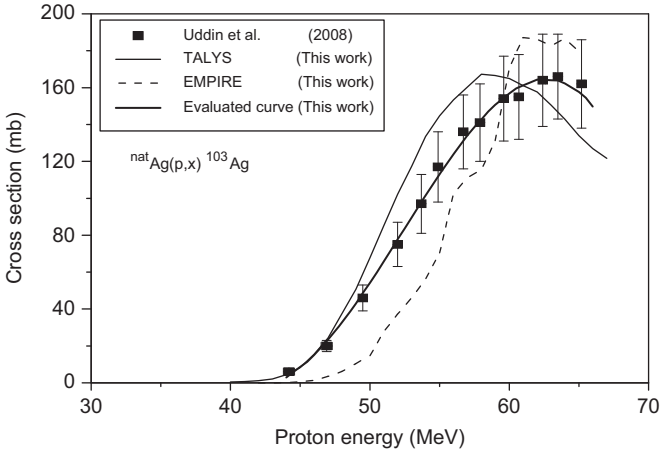

Fig. 11. Experimental data for the ^{nat}Ag(p,x)^{103}Ag reaction in comparison with the results of nuclear model calculations. The evaluated curve is given as a solid line.

Since all measurements have been recently done using standard decay and flux monitor data, no normalization was done. The cross-sections of the ^{nat}Pd(α,x)^{103}Ag and ^{nat}Cd(p,x)^{103}Ag reactions are small; so we neglected those processes. Out of the remaining three reactions, the ^{nat}Ag(p,x)^{103}Ag process has high cross-section. It has been reported that about 70% of the total ^{103}Pd is formed via the decay of ^{103}Ag (Uddin et al., 2008). Similarly the ^{nat}Pd(p,x)^{103}Ag process also has high cross-section. The cross-section data of the latter two processes suggest that the ^{103}Ag→^{103}Pd precursor route could be interesting, but we feel that it would not be of much practical value in the production of ^{103}Pd. A detailed discussion regarding that aspect is given below separately (see Section 10).

Regarding the cross-sections for the ^{nat}Pd(p,x)^{103}Ag process, we adopted the recent data reported by Tárkányi et al. (2009). The experimental data on ^{nat}Ag(p,x)^{103}Ag process (Uddin et al., 2008) are given in Fig. 11. The nuclear model calculations were done using the codes EMPIRE 2.19 and TALYS, which are more suitable in the intermediate energy range. The calculational results are also shown in Fig. 11. They reproduce the experimental data only partly. In some

Table 8
Recommended sets of data for the $^{nat}Ag(p,x)^{103}Ag$ reaction.

Energy (MeV)	σ(mb)	95% confidence limits		Energy (MeV)	σ(mb)	95% confidence limits	
		Lower	Upper			Lower	Upper
44.0	2.9	2.5	4.6	56.0	124	107	140
45.0	8.6	6.5	11.5	57.0	134	116	151
46.0	15.2	11.7	19.5	58.0	143	123	162
47.0	23.3	18.2	28.6	59.0	151	130	171
48.0	32.8	26.4	39.2	60.0	157	135	180
49.0	43.0	35.4	50.7	61.0	161	137	186
50.0	54.2	45.1	62.7	62.0	164	138	191
51.0	65.8	55.4	75.5	63.0	164	138	195
52.0	77.7	66.0	88.5	64.0	162	134	195
53.0	89.7	76.7	102	65.0	158	127	194
54.0	102	87.3	115	66.0	150	119	190
55.0	113	97.4	127				

energy regions the calculations and experimental data agree whereas in several other regions the calculational values are either overestimates or underestimates. On the other hand, the agreement between experiment and theory may be regarded as satisfactory, considering that the formation of ^{103}Ag involves several complex reaction channels. As in all other cases, we did polynomial fitting to the ratio (measured/model calculated) data, but only for two nuclear model codes mentioned above. No data point was found beyond the 3σ limit, so all the data were used for evaluation. The recommended sets of data were generated, and upper and lower 95% confidence limits were determined for the best estimation of uncertainty in the recommended values. The recommended sets of data are given in Table 8.

9. Discrepancy in determination of ^{103}Pd activity

The determination of the absolute radioactivity of ^{103}Pd poses some problem since it does not emit any easily detectable radiation, e.g. a β^- particle or a positron, which can be detected by β-ray spectroscopy, and a γ-ray emitted with the energy 357.4 keV has very weak intensity (0.022%). Although the K_α and K_β X-rays of energies 20.2 and 22.7 keV, respectively, are sufficiently strong, their detection and use in absolute activity determination are rather subtle. While investigating the $^{103}Rh(p,n)^{103}Pd$ reaction most of the early measurements on the ^{103}Pd activity were done via gross X- and γ-ray counting. In recent years, however, measurements have been reported on this reaction using both high-resolution γ-ray spectrometry and high-resolution X-ray spectrometry (Hermanne et al., 2000; Sudár et al., 2002) and the results were found to be discrepant, the data obtained by γ- ray spectrometry being about 20% higher. The same observation was made while studying the $^{103}Rh(d,2n)^{103}Pd$ reaction (Hermanne et al., 2002a, b). We considered four possible reasons for the discrepancy:

(a) the reported intensity of the 357.4 keV γ-ray may be faulty, especially because it is so low;
(b) the self-absorption corrections made for X-rays in Rh foils (Hermanne et al., 2000, 2002a, b; Sudár et al., 2002) may be overestimates;
(c) the efficiency of the low-energy detector used in X-ray spectroscopy may be rather uncertain, since the available experience to date is rather limited;
(d) the reported intensity of the Rh K-X-rays may be in error.

We discuss these points in some detail. The intensity of the 357.4 keV γ-ray is low but still it appears to be correct. A recent measurement (Popov et al., 2004) confirmed the intensity ratio of this γ-ray to two other weak γ-rays of ^{103}Pd. The self-absorption correction entails a random uncertainty. Since Rh foils of different thicknesses were used and since the results from two independent groups (Hermanne et al., 2000; Sudár et al., 2002) are in agreement, self-absorption correction should not be the source of discrepancy. The same applies to the efficiency of the X-ray detector. The identical results obtained by the above-mentioned two different groups rule this out as a possible source of discrepancy. Regarding the intensity of the Rh K X-rays, the ratio K_α/K_β of X-rays has been recently confirmed (Popov et al., 2004), but the total intensity of 77.0% appears to be doubtful. The new value suggested by Berlyand et al. (2002), which is about 20% lower, would remove the discrepancy in the cross-section data (see also Tárkányi et al., 2009). However, it will have strong repercussions on the dosimetry related to brachytherapy with ^{103}Pd. Thus, till further confirmation of the X-ray intensity, the discrepancy between the cross-section data obtained via γ-ray spectrometry and X-ray spectrometry remains unsolved.

It is instructive to consider the cross-section data for the formation of ^{103}Pd from target elements other than Rh. Measurements have been done on $^{nat}Pd(p,x)^{103}Pd$ (Hermanne et al., 2004), $^{nat}Pd(d,x)^{103}Pd$ (Hermanne et al., 2004), $^{nat}Pd(\alpha,x)^{103}Pd$ (Hermanne et al., 2005), $^{nat}Ag(p,x)^{103}Pd$ (Fassbender et al., 1999; Uddin et al., 2005, 2008), and $^{nat}Cd(p,x)^{103}Pd$ (Tárkányi et al., 2006, 2007, 2009) reactions but, unfortunately, only via γ-ray spectrometry, except for the $^{nat}Ag(p,x)^{103}Pd$ process, where both γ-ray and X-ray spectrometry were used. It has been shown above that in the case of Ag as target, the X-ray and γ-ray data are in agreement (Fig. 1), although the limited data have relatively large uncertainties. The above-mentioned discrepancy is thus possibly associated with Rh as the target.

It should also be pointed out that a few measurements done on the $^{103}Rh(p,n)^{103}Pd$ reaction using assay of the emitted neutrons (Albert, 1959; Hansen and Albert, 1962; Johnson et al., 1960) give cross-section values nearer to the data obtained via X-ray spectrometry. The discrepancy in the data obtained via γ-ray spectrometry thus appears to be due to an overestimate of the 357.4 keV γ-ray peak. Sudár et al. (2002) discussed this problem and speculated the presence of some trace impurity in Rh target that gives an activation product emitting a γ-ray in the vicinity of the 357 keV γ-line. They also postulated that the effect of the impurity is more pronounced in the energy region below 15 MeV, i.e. the contributing process is a low-energy reaction. The Rh foils used in the three major works (Hermanne et al., 2000, 2002; Sudár et al., 2002) were >99.9% pure. The level of impurity was thus ≤1000 ppm. In one work (Hermanne et al., 2002a, b) the detected impurities Fe, Ru, and In, were reported by the supplier to amount to 180 ppm. Now if some undetected impurity, e.g. Pt (a transition element like Rh) would be present at a level of about 100 ppm, it would lead via a low-energy (p,n) reaction to ^{196}Au, which emits a γ-ray of energy 356 keV. The magnitude of the (p,n) cross-section on Pt is expected to be about three times smaller than that for Rh. A simple calculation shows that the contribution of the impurity to the peak area around the 357 keV γ-line may amount to about 10%. Thus performing cross-section measurements on the $^{103}Rh(p,n)^{103}Pd$ reaction using Rh foils of ultra-high purity is suggested, or separating ^{103}Pd radiochemically (to isolate it from non-isotopic impurities like ^{196}Au) from the presently used Rh foils. Anyway, further clean experiments are necessary to solve the discrepancy.

10. Application of the evaluated data: calculation of integral yields and comparison of potential production routes

An analysis of the available experimental information on the excitation functions of the reactions $^{nat}Ag(p,x)^{103}Pd$, $^{103}Rh(p,n)^{103}Pd$, $^{103}Rh(d,2n)^{103}Pd$, $^{100}Ru(\alpha,n)^{103}Pd$, $^{101}Ru(\alpha,2n)^{103}Pd$, and $^{102}Ru(^3He,2n)^{103}Pd$, and their validation using three nuclear model

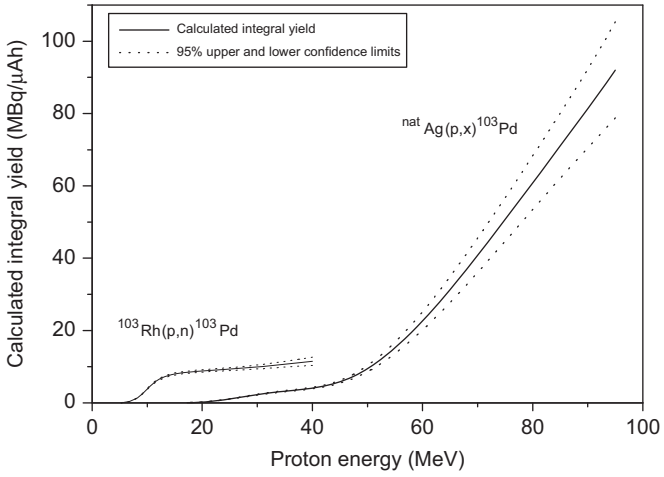

Fig. 12. Calculated integral yield of the $^{nat}Ag(p,x)^{103}Pd$ and the $^{103}Rh(p,n)^{103}Pd$ reaction.

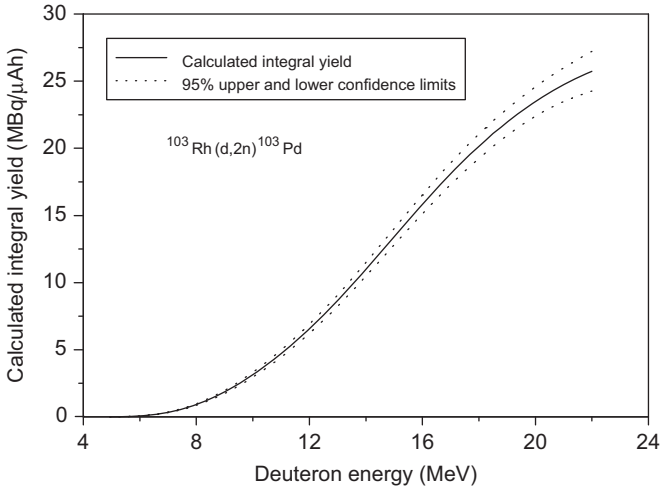

Fig. 13. Calculated integral yield of the $^{103}Rh(d,2n)^{103}Pd$ reaction.

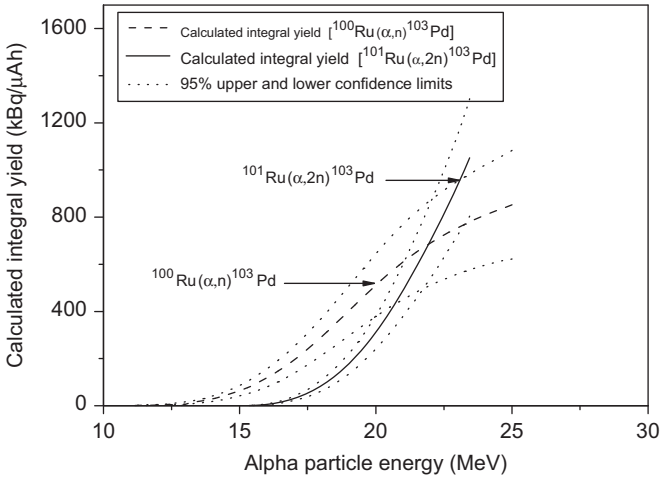

Fig. 14. Calculated integral yield of the $^{100}Ru(\alpha,n)^{103}Pd$ and the $^{101}Ru(\alpha,2n)^{103}Pd$ reaction.

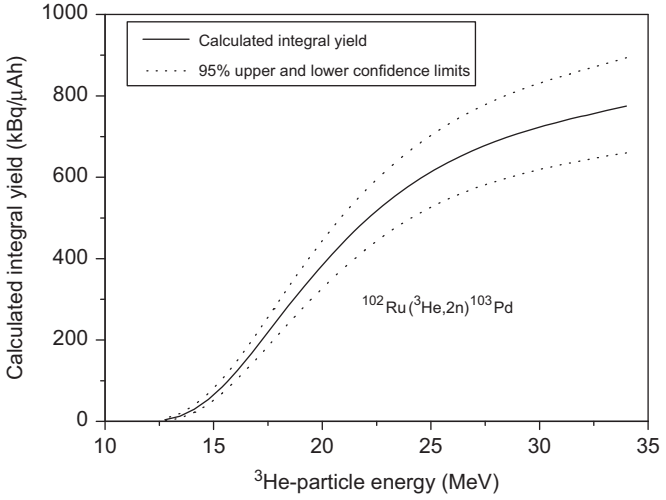

Fig. 15. Calculated integral yield of the $^{102}Ru(^3He,2n)^{103}Pd$ reaction.

calculational codes, namely STAPRE, EMPIRE, and TALYS, has led to recommended data sets for those reactions. Those data could now be confidently used for calculation of integral yield of ^{103}Pd in a given reaction over a certain energy range. We give the calculated yields for the above six reactions in Figs. 12–15 together with the 95% confidence limits. These yield values should be, in general, more accurate than the ones reported by authors from their own individual measurements. The calculated integral yields for (p,n) and (d,2n) reactions agree with the experimental yields reported by Dmitriev (1986) up to 12 MeV. For higher energies the calculated values are about 5–10% lower than the Dmitriev (1986) values. This is somewhat surprising but, without knowing the experimental details of old yield measurements, it is not possible to look for the reason of the deviation. Our calculated integral yields for the $^{103}Rh(p,n)^{103}Pd$ reaction up to 40 MeV are 8% higher than the recommended yields in the ongoing CRP of the IAEA (Qaim et al., 2009). For the $^{103}Rh(d,2n)^{103}Pd$ reaction up to 20 MeV, our yield values are 9% higher than the CRP values.

The cyclotron production of a medical radionuclide demands consideration of cross-section data not only of the desired reaction (to be able to calculate the integral yield) but also of other competing reactions leading to possible disturbing radioactive impurities. The palladium radionuclides other than ^{103}Pd formed over the energy regions covered in this work are generally short lived. In the case of $^{nat}Ag(p,x)^{103}Pd$ process, only the somewhat longer-lived impurity $^{100}Pd(T_{1/2} = 3.7\,d)$ needs to be considered.

A comparison of all the reaction yields shows that the $^{nat}Ag(p,x)^{103}Pd$ process at about 70 MeV leads to the highest ^{103}Pd yield but the level of ^{100}Pd impurity amounts to about 50% (cf. data by Uddin et al., 2005) and a waiting time of about 25d may be necessary to decrease its contribution to $<1\%$ of ^{103}Pd. Although the yield of ^{103}Pd increases beyond 70 MeV, higher incident proton energies should be avoided since the level of ^{100}Pd would also increase considerably. The limitation of lower energy cyclotron favours the $^{103}Rh(p,n)^{103}Pd$ or the $^{103}Rh(d,2n)^{103}Pd$ reaction. Since, at low and medium energy, commercial cyclotrons proton beams of much higher intensity are available than deuteron beams, presently the $^{103}Rh(p,n)^{103}Pd$ reaction constitutes the method of choice. In this connection the role of chemistry also needs to be considered. Whereas in the $^{nat}Ag(p,x)^{103}Pd$ process a chemical separation of ^{103}Pd is absolutely mandatory, in the $^{103}Rh(p,n)^{103}Pd$ reaction, the irradiated material can be used directly via brachytherapy, provided the proton energy is kept below 12 MeV to avoid the formation of the long-lived $^{102m,g}Rh$. On the other hand, if higher proton energy is used, or if the Auger electrons are to be utilized for therapeutic purpose, the no-carrier-added ^{103}Pd must be chemically separated from ^{103}Rh and the

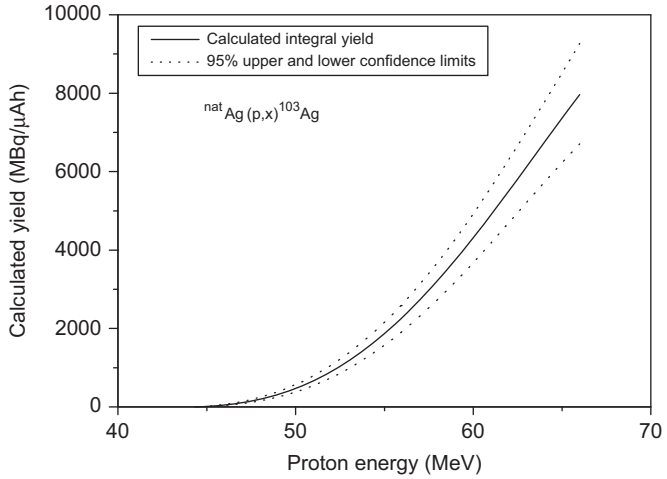

Fig. 16. Calculated integral yield of the $^{nat}Ag(p,x)^{103}Ag$ reaction.

matrix activity, and a thin source must be prepared. Batch yields of ^{103}Pd generally achieved via this route amount to more than 200 GBq.

The $^{103}Ag \rightarrow {}^{103}Pd$ precursor route has been optimistically suggested for production of ^{103}Pd (Hermanne et al., 2004, 2005; Tárkányi et al., 2009). We are, however, skeptical on the basis of the following consideration. The yield of ^{103}Ag calculated from the $^{nat}Ag(p,x)^{103}Ag$ reaction data is shown in Fig. 16. Since the half-life of ^{103}Ag is only 1.1 h, the maximum irradiation time could be 5h, during which it will reach saturation. The batch yield over $E_p = 65 \rightarrow 45$ MeV achieved would then be about 15,000 MBq/μA. A higher energy range would not add much to the yield since the reaction cross-section decreases rapidly beyond 65 MeV (cf. Fig. 11). Assuming the time of separation as 1h and the chemical yield of about 70%, the batch yield of ^{103}Ag would be reduced to about 5000 MBq/μA. This corresponds to a yield of about 13.5 MBq/μA of ^{103}Pd. Since modern accelerators in the energy range under consideration often deliver beam currents of around 100 μA, the total batch yield of ^{103}Pd would amount to about 1.4 GBq. A similar calculation for the $^{nat}Pd(p,x)^{103}Ag$ process based on the data of Hermanne et al. (2004) and Tárkányi et al. (2009) over the whole investigated energy range of $E_p = 65 \rightarrow 16$ MeV gave a value of about 23,000 MBq/μA for ^{103}Ag. The chemical separation of radiosilver from a thick palladium target (about 6 gcm^{-2}) would need much more time than in the case of a silver target, so that the practically achievable batch yield of ^{103}Ag may not be more than 5000 MBq/μA. The total batch yield of ^{103}Pd (under the same assumptions as for a silver target) would then again amount to about 1.4 GBq. Considering the efforts involved in rapid chemical processing of both ^{nat}Pd and ^{nat}Ag targets, the yield of ^{103}Pd achieved via the $^{103}Ag \rightarrow {}^{103}Pd$ precursor route is too small.

It may be pointed out that for the silver target the route $^{103}Ag \rightarrow {}^{103}Pd$ is not essential since the cumulative route $^{nat}Ag(p,x)^{103}Pd$ is much more effective for production of no-carrier-added ^{103}Pd (see Section 4.1). For palladium target, however, the precursor route is mandatory; the effort involved is high and the ^{103}Pd yield rather low. The advantage of the $^{103}Ag \rightarrow {}^{103}Pd$ route, on the other hand, for both silver and palladium targets, could be the resulting high radionuclidic purity of ^{103}Pd. Even at a high incident particle energy of 100 MeV the separated ^{103}Pd would be free of ^{100}Pd since its precursors $^{100m,g}Ag$ ($T_{1/2} = 2.0$ min, 2.3 min) would decay out rapidly during the chemical separation of ^{103}Ag.

It should be mentioned that the reactions $^{100}Ru(\alpha,n)^{103}Pd$ and $^{102}Ru(^3He, 2n)^{103}Pd$ are of little practical significance since the expected yields of ^{103}Pd are very low. On the other hand, the results of nuclear model calculations suggest that the $^{101}Ru(\alpha,2n)^{103}Pd$ reaction may be promising and at energies around 35 MeV the ^{103}Pd production yield would exceed 2 MBq/μA h. If long and high current irradiations are done (e.g. for 50 h at 30 μA), the batch yield of ^{103}Pd may amount to about 3 GBq. This is not high, but could constitute a useful proposition if α-irradiations could be done in a parasitic position for a few hundred hours.

11. Conclusion

This work presents the first thorough evaluation of all potentially useful charged-particle data available to date for the production of ^{103}Pd in no-carrier-added form. Comprehensive and extensive nuclear model calculations using the codes STAPRE, EMPIRE 2.19, and TALYS in support of the statistical fitting procedure showed the limitations of several experimental data. The recommended sets of data should be useful for optimization of various routes for production of ^{103}Pd at an accelerator or a cyclotron. It should, however, be reiterated that the recommended data are based on X-ray spectrometry. If the intensity of the X-rays would change, all the data will have to be renormalized.

Acknowledgements

This work has been performed under the PIN no. 041-211338-P-103, Higher Education Commission (HEC), Islamabad, Pakistan. M. Hussain gratefully acknowledges the hospitality of the Institute of Experimental Physics, University of Debrecen, Debrecen, Hungary. He also thanks the IAEA for supporting his participation in the workshop on nuclear model calculations (2008) in Vienna.

References

Albert, R.D., 1959. (p,n) cross section and proton optical model parameters in the 4 to 5.5 MeV energy region. Phys. Rev. 115, 925–927.

Becchetti Jr., F.D., Greenlees, G.W., 1969. Nucleon-nucleus optical model parameters, $A > 40$, $E < 50$ MeV. Phys. Rev. 182, 1190–1209.

Belgya, T., Bersillon, O., Capote Noy, R., Fukahori, T., Zhigang, Ge., Goriely, S., Herman, M., Ignatyuk, A.V., Kailas, S., Koning, A.J., Obložinský, P., Plujko, V., Young, P.G., 2006. Handbook for Calculations of Nuclear Reaction Data. RIPL-2, IAEA-TECDOC-1506, pp. 1–171.

Berlyand, T.P., Grigor'ev, E.I., Orlov, V.P., 2002. Ionizing radiation measurements: measurement of relative intensity of ^{103}Pd photon radiation. Meas. Tech. 45, 974–977.

Bersillon, O., 1981. SCAT 2: Un programme de modele optique spherique. Centre d'Etudes de Bruyéres-le-Châtel Report, CEA-N-2227.

Blaser, J.P., Boehm, F., Marmier, P., Scherrer, P., 1951. Anregungsfunktionen und Wirkungsquerschnitte der (p,n) Reaktion (II). Helvetica Phys Acta 24, 441.

Capote, R., Bêták, E., Carlson, B.V., Choi, H.D., Ignatyuk, A., Menapace, E., Nortier, F.M., Qaim, S.M, Scholten, B., Shubin, Y.N., Sublet, J.C., Tárkányi, F.T., 2008. IAEA coordinated research programme: nuclear data for the production of therapeutic radionuclides. In: Bersillon, O., Gunsing, F., Bauge, E., Jacqmin, R., Leray, S. (Eds.), Proceedings of the International Conference on Nuclear Data for Science and Technology, Nice, France, 2007. CEA, Paris, pp. 1367–1370.

Collé, R., Kishore, R., Cumming, J, 1974. Excitation functions for (p,n) reactions to 25 MeV on ^{63}Cu, ^{65}Cu and ^{107}Ag. Phys. Rev. C 9, 1819.

Dmitriev, P.P., 1986. Radionuclide yield in reactions with protons, deuterons, alpha particles and helium-3. IAEA, INDC (CCP) -263/G+CN+SZ, pp. 105–106.

Dilg, W., Schantl, W., Vonach, H., Uhl, M., 1973. Level density parameters for the back-shifted Fermi gas model in the mass range $40 < A < 250$. Nucl. Phys. A 217, 269–298.

Egidy, T.V., Bucurescu, D., 2005. Systematics of nuclear level density parameters. Phys. Rev. C 72, 044311.

EXFOR database. 2009. 〈http://www-nds.iaea.org/exfor/exfor.htm〉.

Fassbender, M., Nortier, F.M., Schroeder, I.W., Van der Walt, T.N., 1999. The production of ^{103}Pd via the $^{nat}Ag(p,x)^{103}Pd$ nuclear process. Radiochim. Acta 87, 87–91.

Gilbert, A., Cameron, A.G.W., 1965. A composite nuclear level density formula with shell corrections. Can. J. Phys. 43, 1446–1498.

Gul, K., Hermanne, A., Mustafa, M.G., Nortier, F.M., Obložinský, P., Qaim S.M., Scholten, B., Shubin, Yu., Takács, S., Tárkányi, F., Zhuang, Y., 2001. Charged particle cross section database for medical radioisotopes production: diagnostic radioisotopes and monitor reactions. IAEA-TECDOC-1211, pp. 1–285.

Hansen, L.F., Albert, R.D., 1962. Statistical theory predictions for 5 to 11 MeV (p,n) and (p,p′) nuclear reactions in ^{51}V, ^{59}Co, ^{63}Cu, ^{65}Cu, and ^{103}Rh. Phys. Rev. 128, 291–299.

Harper, P.V., Lathrop, K., Need, J.L., 1961. The thick target yield and excitation function for the reaction ^{103}Rh(p,n)^{103}Pd. ORNL-LR-DWG 51564 124.

Herman, M., Capote, R., Carlson, B.V., Obložinský, P., Sin, M., Trkov, A., Wienke, H., Zerkin, V., 2007. EMPIRE: nuclear reaction model code system for data evaluation. Nucl. Data Sheets 108, 2655–2715.

Hermanne, A., Sonck, M., Fenyvesi, A., Daraban, L., 2000. Study on production of ^{103}Pd and characterization of possible contaminants in the proton irradiation of ^{103}Rh up to 28 MeV. Nucl. Instrum. Methods Phys. Res. B 170, 281–292.

Hermanne, A., Sonck, M., Takács, S., Tárkányi, F., Shubin, Y., 2002a. Deuteron bombardment of ^{103}Rh: a new promising pathway for the production of ^{103}Pd. J. Nucl. Sci. Technol. (Suppl. 2), 1286–1289.

Hermanne, A., Sonck, M., Takács, S., Tárkányi, F., Shubin, Y., 2002b. Study on alternative production of ^{103}Pd and characterization of contaminants in the deuteron irradiation of ^{103}Rh up to 21 MeV. Nucl. Instrum. Methods Phys. Res. B 187, 3–14.

Hermanne, A., Takács, S., Tárkányi, F., Bolbos, R., 2004. Cross section measurements of proton and deuteron induced formation of ^{103}Ag in natural palladium. Radiochim. Acta 92, 215–218.

Hermanne, A., Tárkányi, F., Takács, S., Shubin, Yu.N., 2005. Experimental determination of cross section of alpha-induced reactions on ^{nat}Pd. Nucl. Instrum. Methods Phys. Res. B 229, 321–332.

Hoefnagel, C.A., 1991. Radionuclide therapy revisited. Eur. J. Nucl. Med. 18, 408–431.

Iwamoto, A., Harada, K., 1982. Mechanism of cluster emission in nucleon induced preequilibrium reactions. Phys. Rev. C 26, 1821–1834.

Johnson, C.H., Galonsky, A., Inskeep, C.N., 1960. Cross sections for (p,n) reactions in intermediate weight nuclei. ORNL-2910 Report 25.

Kalbach-Cline, C., 1973. Residual two body matrix elements for preequilibrium calculations. Nucl. Phys. A 210, 590–604.

Koning, A.J., Delaroche, J.P., 2003. Local and global nucleon optical models from 1 keV to 200 MeV. Nucl. Phys. A 713, 231–310.

Koning, A.J., Hilaire, S., Duijvestijn, M.C., 2005. TALYS: comprehensive nuclear reaction modeling. In: Haight, R.C., Chadwick, M.B., Kawano, T., Talou, P. (Eds.), Proceedings of the International Conference on Nuclear Data for Science and Technology, ND2004, September 26–October 1, 2004, Santa Fe, USA. AIP vol. 769, pp. 1154–1159.

Kopecky, P., 1985. Proton beam monitoring via the Cu(p,x)^{58}Co, ^{63}Cu(p,2n)^{62}Zn and ^{65}Cu(p,n)^{65}Zn reaction in copper. Appl. Radiat. Isot. 36, 657.

McFadden, L., Satchler, G.R., 1966. Optical model analysis of the scattering of 24.7 MeV alpha particles. Nucl. Phys. 84, 177–200.

Mukhammedov, S., Vasidov, A., 1984. Determination of rhodium by proton-activation technique using the (p,n) reaction at a cyclotron. Izv. AN UzbSSR Ser. Fiz.-Mat 2, p. 329.

Nesaraja, C.D., Sudár, S., Qaim, S.M., 2003. Cross sections for the formation of ^{69m,g}Zn and ^{71m,g}Zn in neutron induced reactions near their thresholds: effect of reaction channel on the isomeric cross-section ratio. Phys. Rev. C 68, 024603.

Nudat 2.4 database. 2008. 〈http://www-nndc.bnl.gov/nudat2/〉.

Perey, F.G., 1963. Optical model analysis of proton elastic scattering in the range of 9 to 22 MeV. Phys. Rev. 131, 745–763.

Popov, Y.S., Zakharova, L.V., Kupriyanov, V.N., Andreev, O.I., Pakhomov, A.N., Vakhetov, F.Z., 2004. Half-life and photon intensities of ^{103}Pd. Radiochemistry 46, 209–210 (Translated from Radiokhimiya, 46, 193–194.).

Qaim, S.M., 2001. Therapeutic radionuclides and nuclear data. Radiochim. Acta 89, 297–302.

Qaim, S.M., 2004. Use of cyclotrons in medicine. Radiat. Phys. Chem. 71, 917–926.

Qaim, S.M., Capote, R., Bêták, E., Carlson, B.V., Caldeira, A.D., Choi, H.D., Ignatyuk, A.V., Kiraly, B., Menapace, E., Nortier, F.M., Paviotti De Corcuera, Scholten, B., Shubin, Y.N., Sublet, J.C., Tárkányi, F.T., 2009. Production of therapeutic radionuclides. IAEA Technical Report, in print, available from 〈http://www-nds.iaea.org/medportal/〉.

Raynal, J., 2003. ECIS code. Distributed by the NEA data bank, Paris, France.

Skakun, Ye., Qaim, S.M., 2005. Excitation functions of hellion-induced nuclear reactions for the production of the medical radioisotope ^{103}Pd. In: Haight, R.C., Chadwick, M.B., Kawano, T., Talou, P. (Eds.), Proceedings of the International Conference on Nuclear Data for Science and Technology, ND2004, September 26–October 1, 2004, Santa Fe, USA. AIP vol. 769, pp. 1634–1637.

Skakun, Ye., Qaim, S.M., 2008. Measurement of excitation functions of helion-induced nuclear reactions on enriched Ru targets for the production of medically important ^{103}Pd and ^{101m}Rh and some other radionuclides. Appl. Radiat. Isot. 66, 653–667.

Stöcklin, G., Qaim, S.M., Rösch, F., 1995. The impact of radioactivity on medicine. Radiochim. Acta 70/71, 249–272.

Sudár, S., Cserpák, F., Qaim, S.M., 2002. Measurements and nuclear model calculations on proton-induced reactions on ^{103}Rh up to 40 MeV: evaluation of the excitation function of the ^{103}Rh(p,n)^{103}Pd reaction relevant to the production of the therapeutic radionuclide ^{103}Pd. Appl. Radiat. Isot. 56, 821–831.

Sudár, S., Qaim, S.M., 1996. Isomeric cross-section ratio for the formation of ^{58m,g}Co in neutron proton, deuteron and alpha-particle induced reactions in the energy region up to 25 MeV. Phys. Rev. C 53, 2885–2892.

Sudár, S., Qaim, S.M., 2006. Cross sections for the formation of ^{195m,g}Hg, ^{197m,g}Hg and ^{196m,g}Au in alpha and ^{3}He-particle induced reactions on Pt: effect of level density parameters on the calculated isomeric cross section ratio. Phys. Rev. C 73, 034613.

Tárkányi, F., Király, B., Ditrói, F., Takács, S., Csikai, J., Hermanne, A., Uddin, M.S., Hagiwara, M., Baba, M., Ido, T., Shubin, Yu N., Kovalev, S.F., 2006. Activation cross-sections on cadmium: proton induced nuclear reactions up to 80 MeV. Nucl. Instrum. Methods Phys. Res. B 245, 379–394.

Tárkányi, F., Király, B., Ditrói, F., Takács, S., Csikai, J., Hermanne, A., Uddin, M.S., Hagiwara, M., Baba, M., Ido, T., Shubin, Yu.N., Kovalev, S.F., 2007. Activation cross sections on cadmium: deuteron induced nuclear reactions up to 40 MeV. Nucl. Instrum. Methods Phys. Res. B 259, 817–828.

Tárkányi, F., Hermanne, A., Király, B., Takács, S., Ditrói, F., Csikai, J., Fenyvesi, A., Uddin, M.S., Hagiwara, M., Baba, M., Ido, T., Shubin, Y.N., Ignatyuk, A.V., 2009. New cross sections for production of ^{103}Pd; review of charged particle production routes. Appl. Radiat. Isot. 67(9), 1574–1581, doi:10.1016/j.para diso/2009.03.100.

Treytl, W.J., Caretto Jr., A.A., 1966. Study of (p,n) reactions between 100 and 400 MeV. Phys. Rev. 146, 836–840.

Uddin, M.S., Baba, M., Hagiwara, M., Tárkányi, F., Ditroi, F., Takács, S., Hermanne, A., 2006. Experimental studies of the deuteron induced activation cross sections on ^{nat}Ag. Appl. Radiat. Isot. 64, 1013–1019.

Uddin, M.S., Baba, M., Hagiwara, M., Latif, S.K.A., Qaim, S.M., 2008. Excitation functions for the formation of some short-lived products in proton induced reactions on silver. Radiochim. Acta 96, 67–72.

Uddin, M.S., Hagiwara, M., Baba, M., Tárkányi, F., Ditroi, F., 2005. Experimental studies on excitation functions of the proton induced activation reactions on silver. Appl. Radiat. Isot. 62, 533–540.

Uhl, M., Strohmaier, B., 1976. Computer code for particle induced activation cross section and related quantities. Report 76/01 and Addenda to this report, Institute für Radiumforschung and Kernphysik, Vienna.

Wilmore, D., Hodgson, P.E., 1964. The calculation of neutron cross sections from optical potentials. Nucl. Phys. 55, 673–694.